Plasmon-Waveguide Resonance and Impedance Spectroscopy Studies of the Interaction between Penetratin and Supported Lipid Bilayer Membranes

Zdzislaw Salamon,* Göran Lindblom,† and Gordon Tollin*
*Department of Biochemistry and Molecular Biophysics, University of Arizona, Tucson, Arizona 85721 USA; and †Department of Chemistry, Biophysical Chemistry, Umeå University, SE-90187, Umeå, Sweden

ABSTRACT The interaction between the cell-penetrating peptide, penetratin, and solid-supported lipid bilayer membranes consisting of either egg phosphatidylcholine (PC) or a 75/25 mol% mixture of egg PC and palmitoyloleylphosphatidylglycerol has been studied by simultaneously measuring plasmon-waveguide resonance (PWR) spectra and impedance spectra of lipid-peptide mixtures. When penetratin was incorporated into an egg PC + palmitoyloleylphosphatidylglycerol bilayer, PWR measurements showed a hyperbolic increase in the average refractive index and the refractive index anisotropy, with no change in membrane thickness, over a concentration range between 0 and 2 μM peptide. In the case of an egg PC bilayer, a biphasic dependence was observed, with a decrease in average refractive index and anisotropy and no thickness change occurring between 0 and 5 μM peptide, and an increase in membrane thickness occurring between 5 and 15 μM peptide with no further change in the refractive index parameters. For both membranes, the impedance spectroscopy measurements demonstrated that the electrical resistance was not altered by peptide incorporation, whereas a decrease in membrane capacitance occurred with the same concentration dependence as observed in the PWR experiments, although for the PC membrane no further changes in electrical properties were observed in the higher concentration range. A structural interpretation of these results is described, in which the peptide binds electrostatically within the headgroup region of the bilayer and influences the headgroup conformation, amount of bound water, and the lipid-packing density, without perturbing the hydrocarbon core of the bilayer.

INTRODUCTION

In recent years a great deal of interest has been shown in a group of peptides usually referred to as cell-penetrating peptides (CPP; Langel, 2002). These materials originate from either natural or synthetic sources, and although they are water-soluble they are able to spontaneously cross various cell membranes with high efficacy and low lytic activity. The peptides can be linked to a large protein or an oligonucleotide, which may then be carried through the cell membrane. This has led to their being referred to as ''Trojan peptides'' (Derossi et al., 1998). The ability to translocate cargo molecules across the cell membrane allows these peptides to deliver large hydrophilic biomolecules and drugs into the cytoplasmic space of the cell. As a consequence of this, interesting pharmacological applications have been reported; for example, they have been shown to be functional for experimental pancreatic cancer therapy (Hosotani et al., 2002).

One of the most thoroughly studied examples of a CPP is called penetratin, which has the following 16 amino acid sequence: Arg-Gln-Ile-Lys-Ile-Trp-Phe-Gln-Asn-Arg-Arg-Met-Lys-Trp-Lys-Lys (molecular weight = 2246.7). Penetratin is derived from the homeodomain of the *Drosophila* transcription factor Antennapedia (Derossi et al., 1998). Full understanding of the mechanism behind the penetration ability of the peptide has not been obtained, although many recent studies, utilizing a number of different physical techniques, have been devoted to this problem. Significantly, however, Thorén et al. (2000) showed, using fluorescence microscopy, that penetratin translocates across the lipid bilayer of vesicles via a non-pore-forming mechanism. This provides support for a mode of cell penetration involving only peptide-lipid interactions, with no additional structure-specific interactions required such as shape recognition by a receptor protein. Studies of the kinetics of cellular internalization and cargo delivery of cell-penetrating peptides have also been reported (Kilk et al., 2001, Hällbrink et al., 2001).

A number of spectroscopic studies have been published with the purpose of determining the structure of penetratin both in solution and upon binding to lipid bilayers. Thus, penetratin was examined by ^{1}H-NMR and CD spectroscopy in aqueous solutions of increasing concentration of trifluoroethanol (suggested to represent both extracellular matrix-mimetic and membrane-mimetic environments; Czajlik et al., 2002). It was found, not surprisingly, that the peptide displayed helical conformational features in this low dielectric medium. Interestingly, Lindberg and Gräslund (2001) found by high-resolution NMR spectroscopy in a study of penetratin in sodium dodecylsulphate micellar solutions that the peptide positioned itself as a straight helix with its C-terminus deep inside the micelle and its N-terminus near the surface of the surfactant aggregates. How this can be accomplished in a peptide having positive

Submitted September 4, 2002, and accepted for publication November 11, 2002.

Address reprint requests to Gordon Tollin, Dept. of Biochemistry and Molecular Biophysics, University of Arizona, Tucson, AZ 85721. Tel.: 520-621-3447; Fax: 520-621-9288; E-mail: gtollin@u.arizona.edu.

0006-3495/03/03/1796/12 $2.00

charges distributed throughout its structure is not clear. In contrast, investigations by ellipsometry, pulse modulation infra-red reflection absorption spectroscopy, and FTIR of the structure of penetratin interacting with lipid monolayers or bilayers containing various fractions of a charged lipid showed that the conformation of penetratin is an antiparallel β-sheet (Bellet-Amalric et al., 2000; Binder and Lindblom, private communication). It was concluded that penetratin has a hairpin conformation and that it is bound edge-on to the lipid bilayer, exposing its seven positive charges to the negative lipid headgroups on both sides of the molecule. However, the situation might be more complex, inasmuch as it has recently been reported that the conformation of the peptide is dependent on the peptide concentration, being helical at low concentrations and β-sheet at high concentrations (Persson et al., 2001; Magzoub et al., 2002).

With the aim of obtaining a better understanding of how penetratin interacts with lipid bilayers (both with and without net electrical charges), we have utilized a relatively new spectroscopic method, called coupled plasmon-waveguide resonance (CPWR or PWR; Salamon et al., 1997a; Salamon and Tollin, 1999a,b; 2000; 2001a). This technique is able to characterize the optical properties of a single lipid bilayer, deposited within an orifice of a Teflon sheet in contact with a supporting hydrated silica surface on one side and an aqueous solution on the other. Such a lipid membrane has physico-chemical properties that are similar, although not exactly identical, to the classical bilayer lipid membrane or BLM (Mueller et al., 1962; White, 1986; Salamon and Tollin, 2001b). It should also be pointed out that the bilayer contains some dissolved solvent (squalene/butanol in the present case) and is in contact with a so-called plateau-Gibbs border that surrounds the edges of the hole, which it covers, in the Teflon sheet. It is also important to note that the membrane system used in this study is significantly different from all of the lipid systems used in the investigations summarized above, where the interactions of penetratin and other CPPs with lamellar liquid crystalline phases, lipid monolayers, or vesicular solutions were explored.

In the present work, we have also carried out simultaneous impedance spectroscopy measurements of the lipid bilayer/penetratin system. This methodology has recently become a standard procedure for the characterization of the electrical properties of thin film layers and interfaces (Hillebrandt et al., 1999; Gritsch et al., 1998; Plant et al., 1994). It has especially important advantages in investigations of supported lipid bilayer membranes interacting with peptides and protein molecules, for the following two reasons. First, it allows one to measure defect densities in the membrane produced by such interactions with high sensitivity. Second, because the different regions of a supported lipid bilayer system contribute to different frequency domains of the impedance spectra (Hillebrandt et al., 1999), this technique allows one to distinguish between changes occurring at the supporting semiconductor electrode and at the different interfaces lying between the support and the lipid membrane, and changes in bulk membrane characteristics such as capacitance and conductivity. We present here the results of both PWR and electrical impedance measurements of the interactions between penetratin and lipid bilayers with no net charge and with a net negative charge, attempting to make a correlation between the structural changes of the membrane (as revealed by PWR) and the alterations in electrical properties (as revealed by impedance spectroscopy).

EXPERIMENTAL METHODS

Cell construction

The optical and electrical measurements were performed in a modified version of the previously described PWR cell (Salamon et al., 1997a; Salamon and Tollin, 2002), as shown in Fig. 1. This involves placing a thin layer of the semiconductor indium tin oxide (ITO) on the outer surface of the SiO_2/silver layer (Salamon et al., 2002). The process used to deposit the ITO layer and the electrical and optical properties of such a layer have been described elsewhere (Morton and Dinca, 1999). The thickness of the various components of this design allows the ITO layer to function both as a semiconductor electrode and as a part of the optical overcoating for PWR spectroscopy. This permits a single device to be used simultaneously for both plasmon resonance and electrical spectroscopy measurements.

Formation of solid-supported lipid bilayer

Self-assembled solid-supported lipid membranes were prepared according to the method used for formation of freely suspended lipid bilayers (Mueller

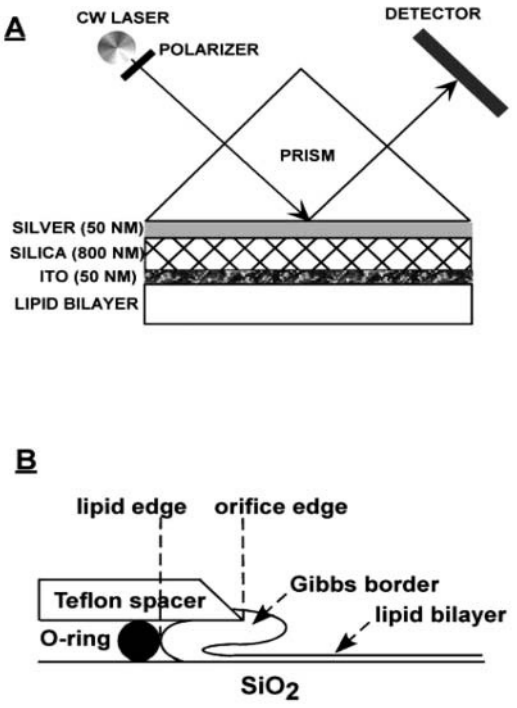

FIGURE 1 (*A*) The PWR resonator design, containing an additional layer of indium tin oxide (ITO) for electrical measurements. (*B*) Shows a schematic representation of the Gibbs border and the lipid bilayer membrane with respect to the Teflon spacer in the sample compartment.

et al., 1962). This involves spreading a small amount of lipid solution across an orifice in a Teflon sheet that separates the thin dielectric film (SiO_2 or SiO_2/ITO) from the aqueous phase (Salamon et al., 1999). The hydrophilic surface of hydrated SiO_2 or ITO attracts the polar groups of the lipid molecules, thus inducing an initial orientation of the lipid molecules, with the hydrocarbon chains pointing toward the droplet of excess lipid solution. The next steps of bilayer formation, induced by adding aqueous buffer into the sample compartment of the PWR cell, involve a thinning process and formation of a plateau-Gibbs border of lipid solution that anchors the membrane to the Teflon spacer. In the present experiments, the lipid films were formed from either a solution containing 20 mg/mL egg phosphatidylcholine (PC) or a mixture of egg PC and 1-palmitoyl-2-oleoyl-*sn*-glycero-3-phospho-rac-(1-glycerol)(sodium salt) (POPG) (75:25 mol/mol) in butanol containing 2.5% (v/v) squalene). The lipids were purchased from Avanti Polar Lipids (Birmingham, AL). All experiments were carried out at ambient temperature using 10 mM Tris buffer containing 0.5 mM EDTA and 10 mM KCl, pH 7.3, in the 2 mL sample cell.

The penetratin peptide was solid-phase synthesized by Dr. Å. Engström at the University of Uppsala, Sweden, and used without further purification.

PWR (CPWR) spectroscopy

Details of the procedures for PWR measurement and data analysis have been described elsewhere (Salamon et al., 1997a,b, 1999; Salamon and Tollin, 1999a). The method is based upon the resonant excitation by polarized light from a CW He-Ne laser ($\lambda = 632.8$ nm), passing through a glass prism under total internal reflection conditions, of collective electronic oscillations (plasmons) in a thin metal film (Ag) deposited on the external surface of the prism which is overcoated with a dielectric layer (SiO_2 or SiO_2/ITO). The resonant excitation of plasmons generates an evanescent electromagnetic field localized at the outer surface of the dielectric film, which can be used to probe the optical properties of molecules immobilized on this surface (for details, see Salamon et al., 1997a, 1999; Salamon and Tollin, 1999a, 2000, 2001a,b). Resonance is achieved by varying the incident angle (α) at a fixed λ. Because the resonance coupling generates electromagnetic waves at the expense of incident light energy, the intensity of totally reflected light is diminished. The reflected light intensity as a function of α results in a PWR resonance spectrum. Resonances can be excited with light polarized either parallel (*p*) or perpendicular (*s*) to the incident plane, resulting in two well-separated spectra (Salamon et al., 1997a), thereby allowing characterization of the molecular organization of anisotropic systems such as biomembranes containing integral peptides or proteins (Salamon et al., 2000a,b; 1996; 1994). Under the experimental conditions employed in this work, the optical parameters obtained with *p*-polarization refer to the perpendicular direction and with *s*-polarization to the parallel direction, relative to the bilayer membrane surface.

PWR spectra can be described by three parameters: α, the spectral width, and the resonance depth. These depend on the refractive index (n), the extinction coefficient (k) and the thickness (t) of the plasmon-generating and emerging media, the latter including a thin film (i.e., a proteolipid membrane in the present case) deposited on the dielectric surface in contact with an aqueous solution. Thin-film electromagnetic theory based on Maxwell's equations provides an analytical relationship between the spectral parameters and the optical properties of these media. This allows evaluation of n, k, and t uniquely for the three media (i.e., the plasmon-generating medium, the proteolipid membrane, and the aqueous solution), by nonlinear least-squares fitting of a theoretical spectrum to the experimental one (for details, see Salamon et al., 1999; 1997b; 2000a,b; Salamon and Tollin, 1999b; 2001b). Inasmuch as the excitation wavelength (632.8 nm) is far removed from the absorption bands of the lipids and peptides used in this work, a k value other than zero reflects a decrease of reflected light intensity due only to scattering resulting from imperfections in the proteolipid film. This effect will not be discussed further in the present work.

It is important to point out that for an anisotropic thin film, such as the proteolipid membrane in the present work, the thickness represents an average molecular length perpendicular to the plane of the film, and will be independent of light polarization. In contrast, the values of the refractive index will be very much dependent on the polarization of the excitation light. Furthermore, for uniaxial anisotropic structures in which the optical axis is parallel to the *p*-polarization direction, the n_p value will always be larger than n_s. This is a consequence of the fact that the measured refractive index of a material is determined by the polarizability of the individual molecules. The latter property describes the ability of a molecule to interact with an external electromagnetic field, and in general is anisotropic with respect to the molecular frame. In the simplified case in which the molecular shape is rod-like (e.g., the phospholipid molecules used in this work), one can assign two different values to the polarizability: the larger one, longitudinal and the smaller one, transverse. If in addition to the anisotropy in molecular shape and polarizability, the system that contains these molecules is ordered such that the long axes of the molecules are parallel, this results in long-range order usually described by the order parameter S. In this situation the values of the polarizability, averaged over the whole system and measured either parallel or perpendicular to the direction of the long axis of the molecules, will be different (i.e., the parallel value will be larger than the perpendicular one). These conditions create an optically anisotropic system, with the optical axis perpendicular to the plane of the proteolipid membrane (Salamon and Tollin, 2001b), and the values of the refractive index measured with two polarizations of light (i.e., parallel, n_p, and perpendicular, n_s to the optical axis) will describe this optical anisotropy (A_n) as follows:

$$A_n = (n_p^2 - n_s^2)/(n_{av}^2 + 2). \quad (1)$$

In this equation, n_{av} is the average value of the refractive index, and for a uniaxial system is given by:

$$n_{av}^2 = 1/3(n_p^2 + 2n_s^2). \quad (2)$$

In summary, the anisotropy in the refractive index reflects both the anisotropy in the molecular polarizability and the degree of long-range order of molecules within the system, and therefore can be used as a tool to analyze structural organization (i.e., molecular orientation; also see Salamon and Tollin 2001b).

Furthermore, as can be seen from the Lorentz-Lorenz relation, the average value of the refractive index is also directly related to the mass density (for details, see Born and Wolf, 1965; Cuypers et al., 1983). Thus, from the thickness of the proteolipid film and the average value of the refractive index one can calculate the surface mass density (or molecular packing density), i.e., mass per unit surface area (or number of moles per unit surface area; Salamon et al., 1999; Salamon and Tollin, 1999a; 2000).

In the present experiments, the plasmon-generating device was calibrated by measuring the PWR spectra obtained from either the bare silica or the bare ITO surface in contact with aqueous buffer with both *p*- and s-polarized light, and then fitting these with theoretical curves. The goal of such a calibration is to obtain the optical parameters of the silica and ITO layers (i.e., refractive indices, extinction coefficients, and thickness) used in these experiments. This provides an input set of data used in analyzing the resonance spectra obtained with the lipid membrane/peptide system deposited on the resonator surface.

Impedance spectroscopy

Impedance spectroscopy measurements were performed over a wide frequency range (1–10^5 Hz) to analyze the electrical properties of the supported lipid bilayer/peptide systems. An impedance analyzer (CH Instruments, USA) was used to apply periodic voltage signals of variable frequency to the electrodes, one of which was connected to the ITO layer and the other placed in the aqueous buffer compartment of the PWR cell. The current response of the system was analyzed in terms of the absolute value of the impedance $|Z|$ and the phase shift angle ϕ. The electrical parameters of individual layers (or interfaces) on the prism surface were determined by fitting the frequency-dependent impedance and phase shift angles of simple

equivalent circuits consisting of resistances, R, and capacitances, C, to the measured data. It is important to emphasize that the various layers of the measuring system, i.e., the ITO semiconductor, the lipid membrane, the buffer (electrolyte), and the interface regions between these layers, predominantly contribute to different frequency domains, which allows one to determine how many different interfaces, represented by individual circuit elements, best fit the experimental spectra. The electrical parameters of the system were determined by fitting both the frequency-dependent impedance and the phase shift of the equivalent circuits to the experimental data. This allowed us to more accurately obtain the two electrical parameters, i.e., resistance, R, and capacitance, C, of the lipid membrane system. The spectra were best fit using an interface model consisting of five equivalent circuits representing the following regions and interfaces: ITO layer, ITO/liquid interface, liquid/BLM interface, BLM layer, and BLM/liquid interface (see Fig. 2 *C*).

To compare results obtained with different membrane systems the specific capacitance (C_B; total membrane capacitance per unit area, or normalized capacitance) together with membrane resistance (R_B; total membrane resistance multiplied by membrane surface area) have generally been used. This requires the measurement of the total bilayer capacitance, C, and resistance, R, as well as the membrane area, B_B. The values of C and R are easily obtained by various standard electrical methods. However, the measurement of membrane area is not a simple task and can be especially difficult in the case of solid-supported lipid membranes. The major reason for this is that such a membrane is anchored to the edge of the orifice in the Teflon spacer by a plateau-Gibbs border of lipid solution. Both the location of the border and its shape, in addition to the orifice dimensions, will determine the surface area of the bilayer. In the case of freely suspended lipid membranes, the Teflon spacer divides the aqueous volume into two parts, resulting in a very symmetrical Gibbs border around the bilayer. In such cases a good approximation of the surface area of the membrane is the surface area of the orifice itself, which can be accurately measured photographically. However, in the case of solid-supported membranes, the Teflon spacer is placed against a solid surface, so there is no longer any symmetry between the two sides of the bilayer (i.e., on one side is a solid surface and on the other an aqueous solution; see Fig. 1 *A*). In addition, because of mechanical constraints and surface roughness there will always be a rather large gap between the solid support and the Teflon spacer, compared to the thickness of the lipid membrane. Under these circumstances neither the annulus (i.e., the Gibbs border) nor the lipid membrane will be situated symmetrically around the edges of the orifice. Instead, both the border and the membrane will be shifted toward the solid support, and in some cases the lipid membrane may even expand underneath the Teflon spacer, resulting in a much larger membrane surface area than that calculated from the orifice dimension (see Fig. 1 *B*). This results, in the present case, in a surface area that lies between 0.5 cm^2 (specified by orifice edge in Fig. 1 *B*), and 1.5 cm^2, if the bilayer extends all the way to the O-ring (this will be discussed further below).

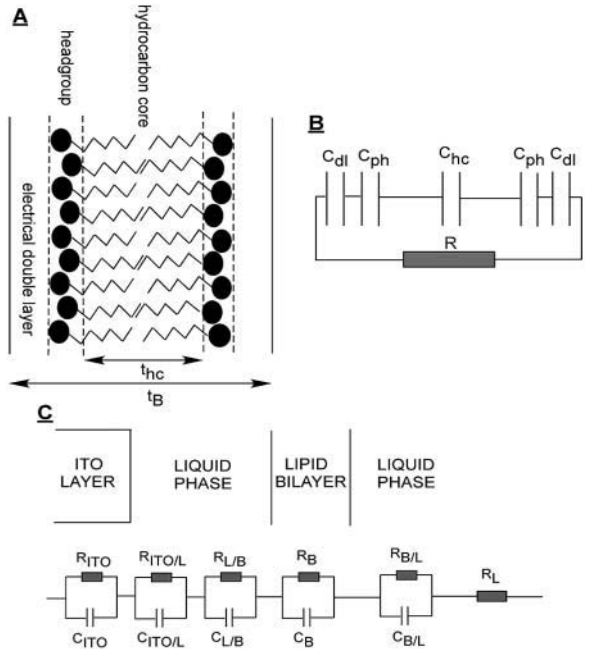

FIGURE 2 A schematic visualization of a lipid bilayer membrane (*A*) containing an electrical double layer, a hydrocarbon core, and two polar headgroup regions, along with its conventionally accepted electrical circuit representation (*B*) consisting of the capacitance of the hydrocarbon core (C_{hc}), two capacitances representing the headgroup interfaces (C_{ph}), and two capacitances representing the electrical double layer (C_{dl}). The capacitances are connected in parallel with a resistance (R), the latter representing the total electrical resistance of the bilayer. In *A*, t_B represents the bilayer thickness as determined from PWR spectroscopy, t_{hc} represents the thickness of the hydrocarbon core of the bilayer. (*C*) shows a schematic view of the ITO/lipid membrane interface. The electrical properties of the interface can be represented by an equivalent circuit consisting of series-connected resistance (R) and capacitance (C) pairs connected in parallel. Each R_C circuit represents one of the five interfaces: ITO; ITO/liquid; liquid/lipid membrane; lipid membrane; and lipid membrane/liquid. R_L represents the resistance of the buffer solution together with all of the wires connecting the system.

Furthermore, the total capacitance, C, is related to the dielectric properties of the capacitor material and is given by the following equation,

$$C_B = \varepsilon_0 \varepsilon B_B / t, \tag{3}$$

where ε_0 and ε are the dielectric coefficients of free space and of the capacitor, respectively, B is the surface area, and t the thickness, of the capacitor. In the case of a lipid bilayer membrane, C_B is determined by the capacitance of the hydrocarbon core, C_{hc}, by the capacitance of the polar headgroups, C_{ph}, and by the capacitance of the electric double layer, C_{dl} (compare with Fig. 2). All three capacitances are in series, i.e., the total capacitance C_B is related to the component capacitances by the following relationship:

$$1/C_B = (1/C_{hc}) + [(2/C_{ph}) + (2/C_{dl})]. \tag{4}$$

Both C_{ph} and C_{dl} are characterized by much higher dielectric coefficient values than that of the nonpolar hydrocarbon core (C_{hc}), and also by a smaller thickness (the polar headgroup region thickness, and the Debye length of the double layer, are both less than the hydrocarbon core thickness; compare with Fig. 2). That results, as Eq. 3 indicates, in much larger values of the capacitance for these regions than for the hydrocarbon core. This means, as is shown by Eq. 4, that C_{hc} makes the major contribution to the total capacitance C_B, although the contributions of both C_{ph} and C_{dl} can still be significant. Furthermore, one can also expect that the values of C_{ph} and C_{dl} will not be exactly the same on both sides of a solid-supported lipid membrane, due to the asymmetric environment of the membrane. In the fitting procedure used in this work we have used the total capacitance C_B normalized per unit surface area. In this context, it is important to point out that PWR measurements result in average values of the membrane thickness, which includes all three parts of the membrane shown in Fig. 2 *A* (t_B) . Thus, the thickness of the hydrocarbon core of the membrane (t_{hc}) is significantly smaller than the value obtained from PWR.

RESULTS AND DISCUSSION

Lipid bilayer membranes

Fig. 3 shows examples of experimental and theoretical PWR spectra for both *s*- and *p*-polarized excitation, obtained with

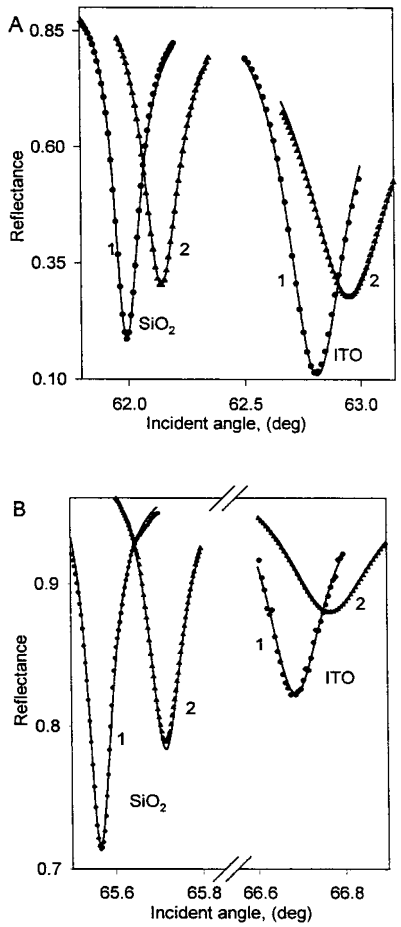

FIGURE 3 Examples of PWR spectra obtained for a supported lipid bilayer using resonators either with ITO (see Fig. 1) or without ITO (with SiO_2 only). (*A*) PWR spectra obtained with an egg PC lipid bilayer membrane formed with 20 mg/mL of egg PC in butanol containing 2.5% squalene and using *p*-polarized light. The buffer composition was 10 mM Tris (pH 7.3), 0.5 mM EDTA, 10 mM KCl. The symbols correspond to experimental data and the solid curves to theoretical fits. Curve 1 was obtained with a bare prism, and curve 2 after deposition of the PC bilayer. (*B*) PWR spectra obtained with the lipid membrane as described in *A* using *s*-polarized light. Symbols and curves as in *A*.

an egg PC bilayer in the absence of penetratin, employing either a cell containing the ITO layer as shown in Fig. 1 or, for comparison purposes, a cell containing only an SiO_2 layer. As is evident, we are able to fit the experimental spectra quite well with theoretical resonance curves, and the presence of the ITO layer does not appreciably degrade the optical performance of the plasmon resonance device. The optical parameters obtained from the theoretical fits for both egg PC and egg PC + POPG bilayers are given in Table 1.

Fig. 4, *A* and *B* shows experimental and theoretical electrical impedance spectra, obtained simultaneously with the optical spectra using the ITO-containing measuring system for both egg PC and egg PC + POPG bilayers. Again, the theoretical fits to the data are quite good. This procedure yields the electrical parameters of the lipid membranes given in Table 1. Fig. 4 *C* shows the frequency dependencies of the impedance and the phase shift parameters (plotted as the ratio between the lipid bilayer and bare prism values). As can be seen, these parameters contribute differently to the frequency spectra, although in both cases the main effects occur below 100 Hz.

The optical parameters obtained with the ITO-coated solid support are in good agreement with those measured with only an SiO_2-coated resonator, as well as with those previously measured for these membrane systems using an SiO_2 PWR resonator (Salamon et al., 2000a,b; 1996; 1994; Salamon and Tollin 2001b). These results clearly indicate that the egg PC + POPG membrane has a higher long-range molecular order (shown by the larger refractive index anisotropy) and a larger thickness than the PC bilayer.

To discuss the results obtained from the electrical measurements it is necessary to consider two factors that influence these values, i.e., the assessment of the lipid membrane surface area and the presence of lipid solvent in the bilayer. As has been pointed out in the previous section, the surface area of a solid-supported lipid bilayer is especially difficult to estimate. Inasmuch as we cannot be certain about the actual value, it is best to present results using both extremes for the membrane surface area (i.e., 0.5 cm^2 and 1.5 cm^2). These are shown in Table 1. It is important to note that, for both approximations, the specific resistance lies between 10^6 and 10^7 ohms cm^2. This demonstrates the very high insulating properties of the membrane, which compares very well with other types of lipid bilayer membranes reported in the literature (Plant et al., 1994; Gritsch et al., 1998). In contrast, the values of the specific capacitance, which range between 1.5 (for the PC + POPG membrane) and 6.8 $\mu F/cm^2$ (for the PC membrane), are significantly higher than usually observed either with freely suspended bilayers (0.4 to 1.0 $\mu F/cm^2$; White, 1986; Plant et al., 1994), or solid-supported membranes (1.6 $\mu F/cm^2$; Plant et al., 1994). There are two ways of accounting for these high values. The first is a trivial explanation based upon the assumption that the lipid film is filled with large pores containing buffer. This will result in a very high dielectric constant and thus high values of specific capacitance. This explanation, however, is inconsistent with both the PWR spectra and the specific resistance values, which should reflect the properties of such a spongy membrane. Thus, the sensitivity of the PWR measurements is high enough to detect the presence of membrane pores with diameters $\geq$100 nm. Furthermore, the specific resistance of a pore-filled membrane should be much smaller than the values observed (between 10^2 and 10^3 ohms, if buffer solution fills the large defects in the membrane; for example, see the values obtained for the aqueous interfaces on both sides of the membrane in the legend to Fig. 4). The second explanation relates to the influence on the membrane capacitance of both the amount of lipid solvent retained

TABLE 1 Values of optical and electrical parameters obtained with lipid membranes consisting of either egg PC, or of 75 mol% egg PC + 25 mol% POPG

		Optical (PWR) results			Electrical results			
					C_B (μF/cm^2)		R_B (ohm cm^2)	
		n_{av}	A_n	t (nm)	0.5 cm^2	1.54 cm^2	0.5 cm^2	1.54 cm^2
SiO_2	PC	1.531 ± 0.001	0.030 ± 0.003	5.1 ± 0.1	–	–	–	–
	PC + PG	1.499 ± 0.001	0.055 ± 0.003	5.8 ± 0.1	–	–	–	–
ITO	PC	1.539 ± 0.001	0.035 ± 0.003	5.1 ± 0.1	6.8 ± 1.5	2.2 ± 1.5	$2 \times 10^6 \pm 10^2$	$7.7 \times 10^6 \pm 10^2$
	PC + PG	1.501 ± 0.001	0.058 ± 0.003	5.9 ± 0.1	4.6 ± 1.1	1.5 ± 1.1	$5 \times 10^5 \pm 10^2$	$1.5 \times 10^6 \pm 10^2$

Electrical parameters have been calculated using two extreme values of the lipid membrane surface area (see above and Fig. 1 *B*).

within the membrane and the above-noted inaccuracy in membrane surface area estimates. There is general agreement that variations in lipid bilayer specific capacitance values reported in the literature result largely from differences in the lipid solvent used to form the membrane. Thus, the presence of residual solvent in the bilayer can significantly alter both the dielectric constant and the membrane structure. As can be seen from Eq. 3, both of these parameters influence the specific capacitance. This is especially important with lipid solvents having a high dielectric constant, as is the case in the present work where butanol has approximately a 10-fold higher value than the lipid membrane hydrocarbon core. In contrast to this, as has been reported previously (Thoma et al., 1996), even relatively large amounts of solvent incorporated within a bilayer membrane will not disrupt the integrity of the membrane and therefore will not change the specific resistance significantly. Using this explanation, and taking into consideration the large differences between the dielectric constant of alkane solvents and butanol, and the uncertainties in membrane surface area, the specific capacitance values obtained in this work (Table 1) are not inconsistent with those previously reported for solid-supported membranes formed with alkane solvents.

As the results in Table 1 also indicate, the specific capacitance obtained using a membrane formed with egg PC is larger than that of an egg PC + POPG membrane. Insight into this difference can be obtained from a comparison of the optical parameters presented in Table 1, which as noted above show that both the optical anisotropy and the thickness of the egg PC membrane are smaller than those of the egg PC + POPG membrane. These results indicate that the latter membrane has more elongated and more ordered fatty acyl chains. A higher degree of order within the membrane due to the presence of the POPG molecules may also indicate less solvent incorporation within the membrane. Therefore, according to Eq. 3, one can conclude that these two factors (i.e., a smaller thickness and more lipid solvent present within the egg PC membrane resulting in a higher value of

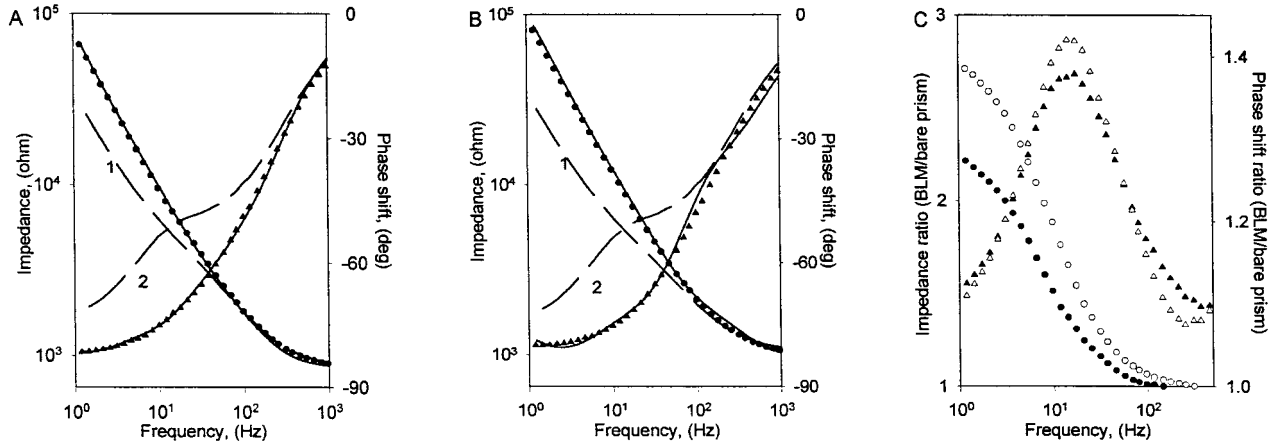

FIGURE 4 Electrical impedance (*circles*) and phase shift (*triangles*) spectra obtained with an ITO-containing resonator as shown in Fig. 1, covered with a lipid membrane formed with 20 mg/mL of egg PC (*A*) or 75 mol% egg PC + 25 mol% POPG (*B*) in butanol containing 2.5% squalene. Dashed lines show the bare prism spectra (no lipid membrane), whereas solid lines are the theoretical fits to the experimental data obtained with the deposited lipid membrane (*closed symbols*). Theoretical fits were obtained with the lipid membrane capacitance and resistance values given in Table 1, and the following parameters for the remaining interfaces (see Fig. 2 *C*) for the PC and PC + POPG membranes, respectively: $R_{ITO} = 4.3 \times 10^5$ and 3.9×10^5; $R_{ITO/L} = 4.0 \times 10^5$ and 8.0×10^5; $R_{L/B} = 1.3 \times 10^3$ and 1.4×10^3; $R_{B/L} = 0.5 \times 10^3$ and 0.8×10^3 ohm cm^2; $C_{ITO} = 2.0$ and 2.0; $C_{ITO/L} = 5.8$ and 4.4; $C_{L/B} = 3.2$ and 3.6; $C_{B/L} = 1.3$ and 1.3 μF/cm^2; and $R_L = 10^3$ and 1.2×10^3 ohm. (*C*) Shows the bilayer/bare prism impedance ratio (*circles*) and phase shift ratio (*triangles*). Closed symbols correspond to the egg PC bilayer whereas open symbols refer to the egg PC + POPG bilayer.

the dielectric coefficient) cause the increased value of the membrane capacitance. It is important to point out that this example clearly demonstrates the value of simultaneous optical and electrical measurements.

Lipid bilayer membranes with penetratin added

PWR spectral changes occurring after addition of aliquots of peptide solution into the aqueous compartment of the sample cell containing a preformed lipid bilayer membrane (made with either egg PC or egg PC + POPG) are illustrated in Fig. 5 *A* by plotting the shifts in the angular position of the resonance spectra, obtained with both *p*- and *s*-polarized exciting light. The changes in the electrical impedance spectra caused by addition of penetratin to both membranes are illustrated by alterations in the amplitude of the phase difference shown in Fig. 5, *B* and *C*. Again, the phase change does not occur uniformly over the entire frequency spectrum, but rather is maximal below 100 Hz.

The PWR results in Fig. 5 *A* clearly indicate two significant differences between the two lipid membranes in their interaction with penetratin. First, the egg PC membrane shows a biphasic pattern of resonance shifts, in contrast with the PC + POPG membrane that yields a simple hyperbolic concentration dependence curve. Second, the interaction between the lipid membrane and the peptide is shifted toward significantly higher penetratin concentrations for the PC membrane (by as much as one order of magnitude) as compared with the PC + POPG bilayer. The latter result is consistent with the net positive electrical charge of penetratin and the net negative electrical charge of the PC + POPG bilayer. We will consider the biphasic character in more detail below.

Theoretical fits to the PWR spectral curves obtained in the experiments of Fig. 5 *A* lead to optical parameter values (i.e., refractive indices, n_p and n_s) and thicknesses, t, that characterize the proteolipid membrane system. In general, PWR spectral changes (i.e., changes in position, depth, and width) obtained with an optically anisotropic membrane are the result of both mass density (i.e., molecular packing density, reflected mainly by the average refractive index values), and structural alterations (reflected by differences between the changes in n_p and n_s; for details see Salamon and Tollin, 1999a,b; 2000, 2001a,b, Salamon et al., 1999). Fig. 6 (for the egg PC membrane) and Fig. 7 (for the egg PC + POPG membrane) show the results of such analyses. In these figures, *A* illustrates the changes of the perpendicular and parallel refractive indices and membrane thickness as a function of penetratin concentration, whereas *B* shows the changes in optical anisotropy and average value of refractive index occurring during the lipid-peptide interaction.

These results provide important insights into the observed differences in spectral shifts (cf. Fig. 5 *A*) between the two membranes in their interaction with penetratin. As Fig. 6 *A* demonstrates, the biphasic pattern of spectral shifts for the egg PC membrane clearly correlates with a sigmoidal pattern of thickness changes, i.e., the penetratin concentration at which the shift direction changes sign in Fig. 5 *A* is approximately the same at which the thickness change begins its sharp rise, whereas no significant thickness change occurs in the region of negative spectral shifts. In contrast, the binding of penetratin to the egg PC + POPG membrane does not produce a significant alteration in the membrane thick-

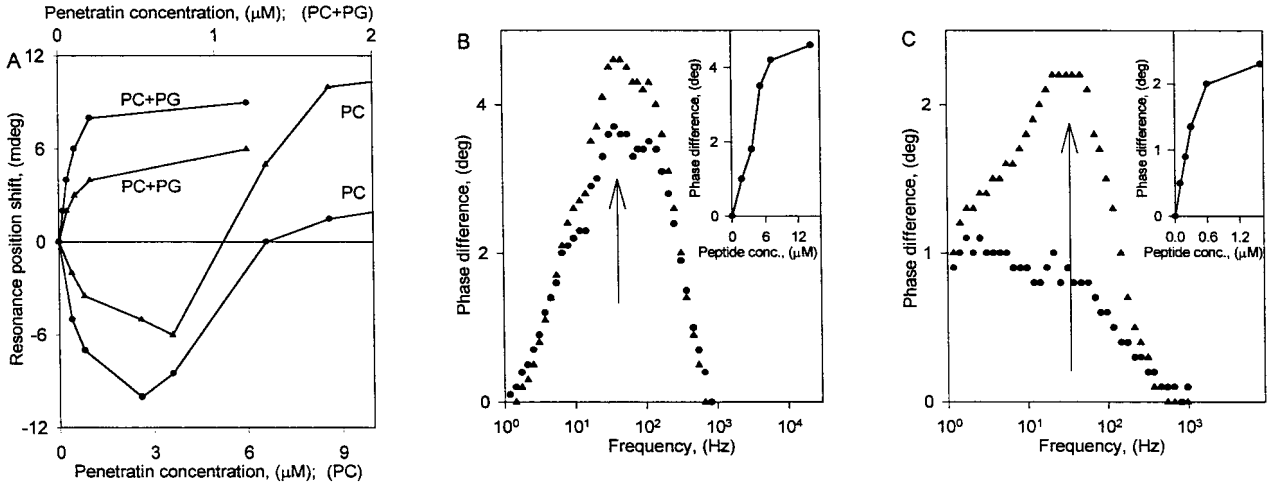

FIGURE 5 (*A*) The PWR spectral maximum position shift (negative values represent a left-hand shift, i.e., a shift to smaller resonance angles) as a function of added penetratin concentration, obtained with both types of lipid membranes using either *p*- (*closed circles*), or *s*-polarized light (*closed triangles*) excitation. *B* and *C* show the phase shift difference between membranes with and without the peptide as a function of frequency, using either an egg PC membrane, *B*, or an egg PC + POPG membrane, *C*. Spectra were obtained with peptide concentrations of either 5.2 μM (*B*; *solid circles*) and 14.4 μM (*B*, *solid triangles*), or 0.2 μM (*C*, *solid circles*) and 1.6 μM (*C*, *solid triangles*). The arrows indicate the frequency at which the phase difference amplitude was determined as a function of peptide concentration and plotted in the inserts in *B* and *C*.

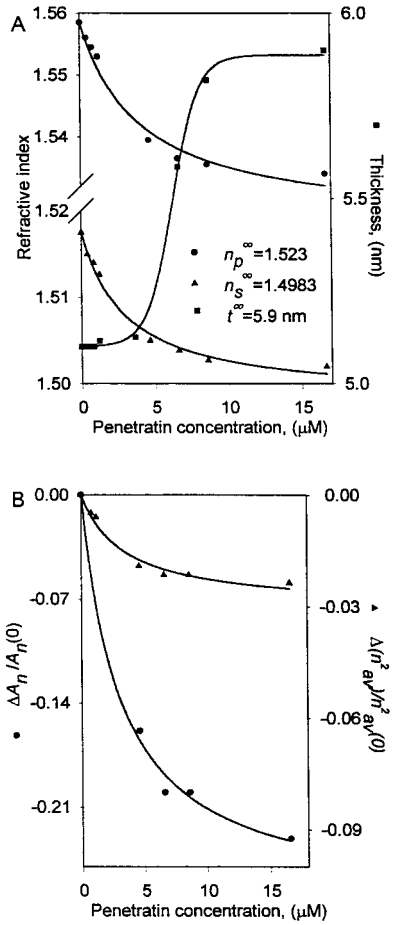

FIGURE 6 PWR results obtained with an egg PC membrane upon penetratin addition. (*A*) Optical parameters (refractive index for either *p*- (*closed circles*) or *s*-polarized light (*closed triangles*) excitation) and thickness (*closed squares*), obtained from the fitting of theoretical spectra to the experimental data, as a function of added penetratin concentration. Included in the figure are the values of these three parameters extrapolated to infinite penetratin concentration. (*B*) Calculated relative changes (i.e., difference between values obtained with and without added penetratin divided by the value obtained without the peptide) of either refractive index anisotropy (A_n, *circles*) or the average refractive index squared (n^2_{av}, *triangles*) as a function of added penetratin, obtained from the optical parameters given in *A*.

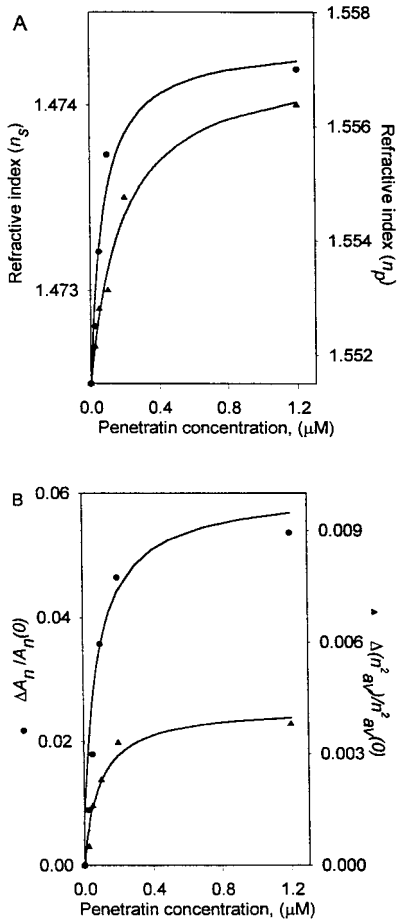

FIGURE 7 PWR results obtained with a 75 mol% egg PC + 25 mol% POPG membrane upon penetratin addition. Parameters defined as in Fig. 6. (*A*) Refractive indices (n_p, *circles*; n_s, *triangles*). (*B*) Relative changes in refractive index anisotropy (*circles*) and average refractive index squared (*triangles*).

ness over the entire concentration range, although it does cause increases in both values of the refractive index (compare Fig. 7 *A* with Fig. 6 *A*). The latter changes lead to an increase in the average value of the refractive index and hence the mass density within the membrane, in sharp contrast to the decrease in this parameter obtained with the PC membrane (compare Figs. 6 *B* and 7 *B*). A similar contrast is observed in the refractive index anisotropy, which measures molecular ordering within the membrane. This parameter increases in the case of the PC + POPG membrane and decreases in the PC membrane during penetratin binding (compare Figs. 6 *B* and 7 *B*). We will discuss the structural interpretation of these differences below.

The analysis of the electrical spectra indicates the following. Most importantly, no measurable change in conductivity (electrical resistance) of either membrane occurs during the binding of penetratin. There are, however, significant changes in the capacitance of both membranes caused by penetratin binding. Fig. 8 illustrates these capacitance changes as a function of peptide concentration. As is evident, the capacitance changes occur in a very similar manner in both types of membranes, and resemble the refractive index and anisotropy alterations presented in Figs. 6 and 7 with respect to the penetratin concentration range within which they occur. For both membranes the capacitance decreases upon peptide binding, reaching values that are 12% and 15% smaller than the original PC and PC + POPG membrane capacitance, respectively. This is despite the fact that both types of membranes demonstrated quite different optical parameter alterations due to the membrane-peptide interaction (as shown in Figs. 6 and 7), indicating different patterns of structural changes in the two lipid bilayers induced by the peptide. Although the fact that the con-

centration dependencies of both the optical and electrical parameters are similar clearly indicates that it is the penetratin interaction with the lipid membrane that causes both the structural and electrical alterations, the results demonstrate that the structural changes observed with PWR cannot be directly associated with the observed alterations in electrical properties. In other words, the changes in electrical properties measured by impedance spectroscopy cannot be caused by changes in the long-range order of the acyl chains, the packing density of the lipid molecules within the bilayer or the thickness of the membrane, inasmuch as all of these parameters change differently in the two membranes. This conclusion, coupled with the fact that there is no measurable change in the conductivity of the membranes due to peptide binding, strongly supports the idea that the penetratin molecules are not creating ion channels or pores across the membrane, nor are they incorporating into the hydrocarbon core of the membrane. This would indicate that the bound peptide molecules must be located somewhere within the polar headgroup region. As a consequence of the charged nature of the peptide and the electrical charges of the headgroups, this would be expected to result in replacing some of the water molecules bound in this region of the bilayer by peptide molecules, thereby lowering the average dielectric constant of the membrane. This in turn would cause a decreased value of the polar headgroup region capacitance, C_{ph} (see Fig. 4). Therefore the total capacitance, C, of the peptide/lipid membrane, compared to that of the lipid bilayer itself, would be lowered by this process, (Eqs. 3 and 4). This is consistent with the results of Fig. 8.

As the optical measurements indicate, the peptide interaction with the PC membrane is more complex than is the case for the PC + POPG membrane, resulting in a biphasic

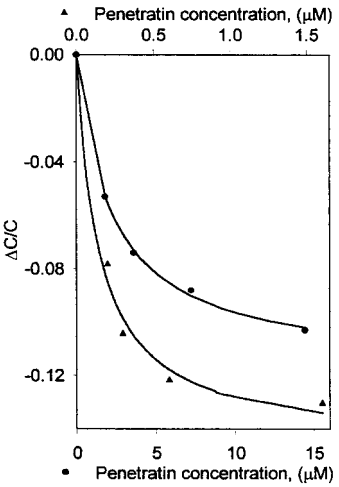

FIGURE 8 Relative changes of lipid membrane capacitance as a function of added penetratin concentration, obtained with either egg PC (*closed circles*) or 75 mol% egg PC + 25 mol% POPG (*closed triangles*) bilayer membranes. C is the capacitance of the bilayer and Δ represents the difference between the capacitance of the membrane containing penetratin and the membrane without added penetratin.

resonance spectral shift (see Fig. 5 *A*). Furthermore, with increasing concentration of peptide, the mass density within the PC membrane decreases, as indicated by a decreasing value of the square of the average refractive index (see Fig. 6 *B*). Such a mass density decrease associated with peptide binding can only occur as a consequence of a decrease in the lipid mass density within the bilayer that overcompensates for the increase of mass produced by the bound peptide, caused by movement of lipid molecules from the bilayer region into the plateau-Gibbs border region. This process can also account for the refractive index anisotropy and the electrical capacitance results, as follows. Movement of lipid molecules out of the bilayer would lead to increased distances between lipid molecules, which in turn would result in a decreased value of the acyl chain long-range order, as measured by the optical anisotropy (Fig. 6 *B*). It would also allow more water molecules to penetrate into the polar headgroup region. According to this view, the net amount of water present within the polar headgroup region of the PC membrane is the result of an increase in water penetration caused by increasing the distance between the lipid headgroups due to peptide incorporation, and a decrease caused by the displacement of water molecules associated with penetratin binding. In addition, one other factor that can affect the total capacitance is the increasing thickness of the PC membrane that occurs with increasing concentration of peptide (see Fig. 6 *A*, and Eqs. 3 and 4). Thus, all three of these processes will contribute to the final value of the total capacitance in the case of the PC membrane, which as shown in Fig. 8 as a net decrease. It is not possible at present to determine whether the thickness increase or the net displacement of water is the dominant factor.

In the case of the egg PC + POPG membrane, however, the mass density increases with increasing concentration of penetratin (Fig. 7 *B*), which taken together with the increased value of the optical anisotropy (Fig. 7 *B*) indicates that, due to peptide insertion into the membrane, the lipid molecules come closer together, decreasing the average distance between them and increasing the average molecular order within the membrane. Presumably, this is a consequence of electrostatic attraction between the penetratin and the negatively charged POPG molecules. This would be expected to result in a net expulsion of water molecules from the polar headgroup region. Inasmuch as there is no measurable membrane thickness change, in this case one can attribute the observed capacitance decrease with increasing peptide concentration (Fig. 8) to such replacement of water molecules by penetratin molecules, leading to a lowering of the average value of the dielectric constant within the polar headgroup region.

SUMMARY AND CONCLUSIONS

It is well established that penetratin, because of its seven positive charges, interacts strongly with lipid membranes

having a negative surface charge density. By utilizing a new modification of the PWR instrument we have been able to investigate the binding mechanism in more detail, by performing measurements of both the optical and the electrical properties of the lipid bilayer in the presence and absence of penetratin. With this new PWR modality it is possible, for the first time, to determine changes in both the electrical resistance, R_B, and the capacitance, C_B, of the bilayer simultaneously with changes in the plasmon resonance spectra. The main results obtained from the different parameters measured in these experiments are summarized in schematic fashion in Fig. 9. Panel *A* visualizes the binding of penetratin to an egg PC + POPG lipid bilayer. Titration of penetratin dissolved in water into the aqueous solution on one side of the supported lipid bilayer results in an increase in the average refractive index, n_{av}, obtained by the PWR optical measurements. This reflects an increase in mass density resulting from peptide binding. As expected, the n_{av} value eventually saturates as the binding sites are filled, at a peptide concentration of less than 1 μM (Figs. 5 and 7). Furthermore, from the PWR optical data it is found that the thickness of the lipid bilayer is constant over this range of peptide concentration and equal to ~5.8 nm. This indicates that the bound peptide does not protrude significantly from the bilayer surface. Like the average refractive index, the anisotropy, A_n, also increases with peptide concentration up to a saturation level of ~1 μM. Thus, the peptide interaction produces a strong increase in the molecular ordering of the system. The seven positive charges of penetratin will bind several (presumably up to seven) of the negatively charged POPG molecules, and will in this way cause an ordering of the lipid headgroups as well as a concomitant ordering of the lipid acyl chains. There is also the possibility that additional POPG molecules residing in the Gibbs border will diffuse

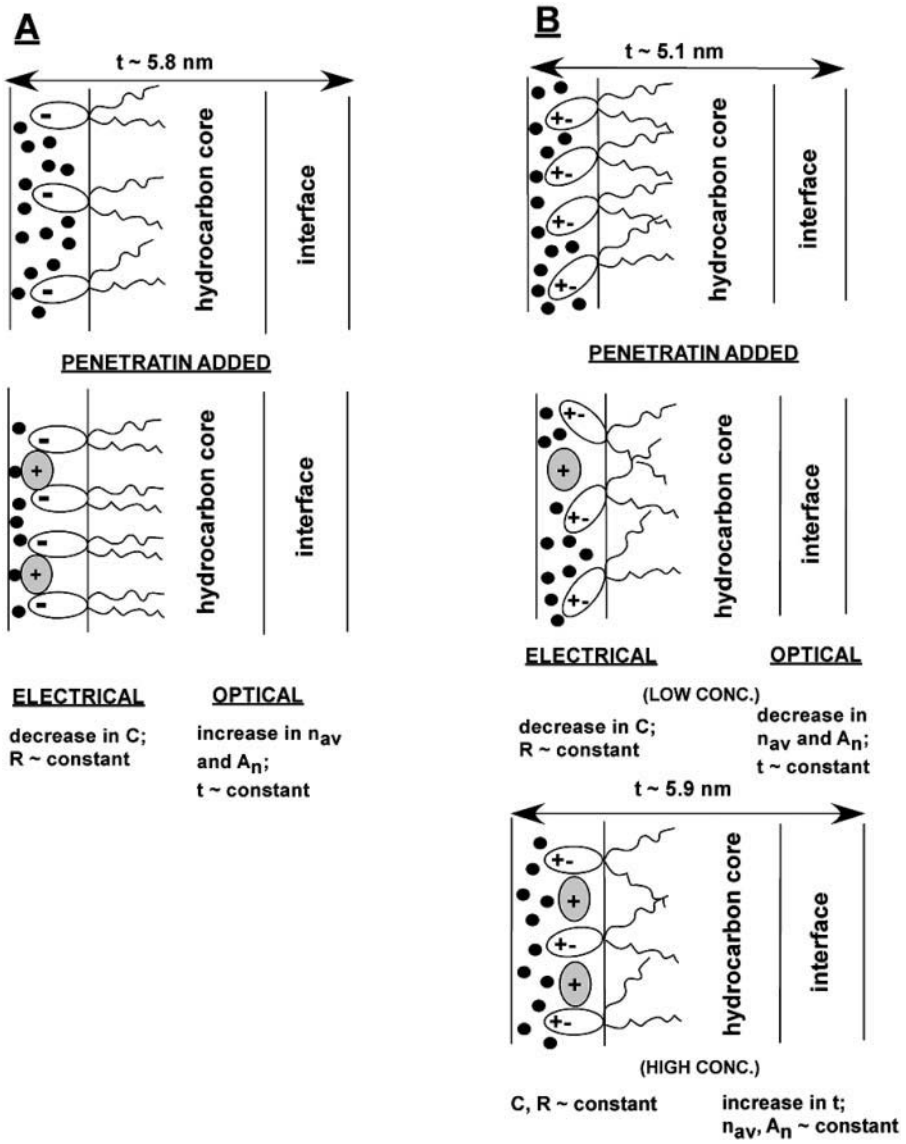

FIGURE 9 Schematic diagrams summarizing the results obtained with both optical and electrical measurements in the absence and presence of added penetratin, either with 75 mol% egg PC + 25 mol% POPG (*A*) or egg PC (*B*) membranes. Only the POPG molecules are depicted in *A*.

into the lipid bilayer so that all the charges of the peptide will be covered, i.e., at a high peptide concentration there will be an increase in the mole fraction of POPG thereby perturbing the initial equilibrium distribution between egg PC and POPG. This will also cause an increase in the observed molecular ordering parameter, inasmuch as the lipid molecules will be more closely packed in the bilayer, as well as in the mass density.

The measured electrical resistance of a lipid bilayer mainly originates from the hydrocarbon core. Upon addition of penetratin, the value of R_B is found to be constant over the entire range of the peptide concentration. This is consistent with the absence of pore or channel formation upon penetratin binding, as has also been indicated from other measurements reported previously (Dupont et al., 2002). The decrease in C_B observed upon peptide binding is consistent with changes in the dielectric medium in the interfacial region of the bilayer (see Fig. 2 for a description of the electrical circuit model of the bilayer). A straightforward interpretation of this observation is that some of the water molecules residing in the lipid headgroup region (the water/headgroup interface has a high dielectric constant, approaching 80) are displaced by the lower dielectric peptide. This is illustrated schematically in Fig. 9 *A*.

Fig. 9 *B* shows how a lipid bilayer composed exclusively of the zwitterionic egg PC is influenced by penetratin interactions. Here, the situation is somewhat more complicated than for the negatively charged POPG bilayer, inasmuch as the observed effects on the bilayer are different at high and low peptide concentration. The measured optical parameters show that in the absence of penetratin the egg PC bilayer is somewhat thinner than the egg PC + POPG bilayer. This is probably because of differences in the headgroup hydration and the fact that, because of the smaller headgroup in POPG, the molecular ordering, i.e., the lipid packing density, is higher for egg PC + POPG than for egg PC. Binding of the peptide at low concentrations results in a decrease in the optical parameters, n_{av} and A_n, which is interpreted to mean that the peptide resides close to the interface causing the electrical repulsion between the positive charges of the peptide and the positive charges of the choline headgroups to push some of the lipid molecules out toward the Gibbs border, thereby decreasing the packing density and the ordering of the lipid molecules in the membrane. Although the electrical resistance in the hydrocarbon core stays unaltered as with egg PC + POPG membranes (implying no channel or pore formation), the capacitance decreases because of a release of some of the water molecules upon binding of penetratin. At higher peptide contents there is an increase in the bilayer thickness to ~5.9 nm, whereas all other parameters are constant, the electrical as well as the optical ones. The most probable interpretation of this observation is that due to the decrease in lipid packing density produced by the initial binding of penetratin, the peptide is able to move deeper into the interfacial region of the lipid headgroups to reach the negative phosphate groups of the egg PC lipid molecules. This straightens out the lipid headgroups, causing the bilayer thickness to increase. However, because of the residual charge repulsion, the lipid packing density, and hence the molecular ordering of the acyl chain region, does not change appreciably. It is important to recall that the binding isotherm for the egg PC bilayer obtained optically also shows a biphasic behavior that saturates at high peptide concentrations.

In summary, our findings are consistent with penetratin having an antiparallel β-sheet hairpin structure (Bellet-Amalric et al., 2000; Binder and Lindblom, private communication), where all the charged amino acids are pointing outwards from both sides of the bent molecule, thereby facilitating an edge-on binding of the peptide to the charged surface of the lipid membrane. It is more difficult to reconcile our data with a peptide having an α-helical structure, as observed in SDS micellar solutions. The present work also shows that penetratin does not penetrate into the hydrophobic core of the lipid membrane causing appreciable disruption of the bilayer structure. Thus, our experimental findings seem to be incompatible with the formation of inverted micelles in the lipid bilayer, as has been suggested to occur by some authors (Dupont et al., 2002). To firmly settle this latter point, however, further studies have to be performed. In addition, to gain more insight into the mechanism of translocation of hydrophilic drugs or larger water-soluble macromolecules by penetratin, extensive investigations of the interactions between lipid bilayers and the peptide, anchored with the appropriate cargo molecule, will have to be carried out.

This work was supported by grants from the National Institutes of Health (GM59630 to G.T. and Z.S.) and the National Science Foundation (MCB-9904753 to G.T. and Z.S.); by a fellowship from the Fulbright Commission (to G.L.); and by Denton Vacuum.

REFERENCES

Bellet-Amalric, E., D. Blaudez, B. Desbat, F. Graner, F. Gauthier, and A. Renault. 2000. Interaction of the third helix of Antennapedia homeodomain and a phospholipid monolayer, studied by ellipsometry and PM-IRRAS at the air-water interface. *Biochim. Biophys. Acta.* 1467:131–143.

Born, M., and E. Wolf. 1965. Principles of Optics. Pergamon Press, New York, New York.

Cuypers, P. A., J. W. Corsel, M. P. Janssen, J. M. M. Kop, W. T. Hermens, and H. C. Hemker. 1983. The adsorption of prothrombin to phosphatidylserine multilayers quantitated by ellipsometry. *J. Biol. Chem.* 258:2426–2431.

Czajlik, A., E. Mesko, B. Penke, and A. Perczel. 2002. Investigation of penetratin peptides. Part 1. The environment dependent conformational properties of penetratin and two of its derivatives. *J. Pept. Sci.* 8: 151–171.

Derossi, D., G. Chassaing, and A. Prochiantz. 1998. Trojan peptides: the penetratin system for intracellular delivery. *Trends Cell Biol.* 8:84–104.

Dupont, E., A. Joliot, and A. Prochiantz. 2002. Penetratins. *In* Cell-Penetrating Peptides. Processes and Applications. U. Langel, editor. CRC Press, Boca Raton, FL. 23–51.

Gritsch, S., P. Nollert, F. Jahnig, and E. Sackman. 1998. Impedance spectroscopy of porin and gramicidin pores reconstituted into supported lipid bilayers on indium-tin-oxide electrodes. *Langmuir*. 14:3118–3125.

Hällbrink, M., A. Floren, A. Elmquist, A. Pooga, T. Bartfai, and U. Langel. 2001. Cargo delivery kinetics of cell-penetrating peptides. *Biochim. Biophys. Acta*. 1515:101–109.

Hillebrandt, H., G. Wiegand, M. Tanaka, and E. Sackmann. 1999. High electrical resistance polymer/lipid composite films on indium tin oxide electrodes. *Langmuir*. 15:8451–8459.

Hosotani, R., Y. Miyamoto, K. Fujimoto, R. Doi, A. Otaka, N. Fukii, and M. Imamura. 2002. Trojan p16 peptide suppresses pancreatic cancer growth and prolongs survival in mice. *Clin. Cancer Res*. 8:1271–1276.

Kilk, K., M. Magzoub, M. Pooga, L. E. G. Eriksson, U. Langel, and A. Gräslund. 2001. Cellular internalization of cargo complex with a novel peptide derived from the third helix of the islet-1 homeodomain. Comparison with the penetratin peptide. *Bioconj. Chem*. 12:911–916.

Langel, U. 2002. Cell-Penetrating Peptides. Processes and Applications. CRC Press, Boca Raton, Florida.

Lindberg, M., and A. Gräslund. 2001. The position of the cell penetrating peptide penetratin in SDS micelles determined by NMR. *FEBS Lett*. 497:39–44.

Magzoub, M., L. E. G. Eriksson, and A. Gräslund. 2002. Conformational states of the cell-penetrating peptide penetratin when interacting with phospholipid vesicles: effects of surface charge and peptide concentration. *Biochim. Biophys. Acta*. 1563:53–63.

Morton, D. E., and A. Dinca. 1999. Ion-assisted deposition of E-gun evaporated ITO films at low substrate temperatures. *In* 42nd Annual Technical Conference Proceedings, Society of Vacuum Coaters, Chicago, IL. 15–22.

Mueller, P., D. O. Rudin, H. T. Tien, and W. C. Wescott. 1962. Reconstitution of cell membrane structure in vitro and its transformation into an excitable system. *Nature*. 194:979.

Persson, D., P. E. G. Thorén, and B. Nordén. 2001. Penetratin-induced aggregation and subsequent dissociation of negatively charged phospholipid vesicles. *FEBS Lett*. 505:307–312.

Plant, A. L., M. Gueguetchkeri, and W. Yap. 1994. Supported phospholipid/alkanethiol biomimetic membranes: insulating properties. *Biophys. J*. 67:1126–1133.

Salamon, Z., M. F. Brown, and G. Tollin. 1999. Plasmon resonance spectroscopy: probing molecular interactions within membranes. *Trends Biochem. Sci*. 24:213–219.

Salamon, Z., S. Cowell, E. Varga, H. I. Yamamura, V. J. Hruby, and G. Tollin. 2000a. Plasmon resonance studies of agonist/antagonist binding to the human δ-opioid receptor: new structural insights into receptor-ligand interactions. *Biophys. J*. 79:2463–2474.

Salamon, Z., G. Lindblom, L. Rilfors, K. Linde, and G. Tollin. 2000b. Interaction of phosphatidylserine synthase from *E. coli* with lipid bilayers: coupled plasmon-waveguide resonance spectroscopy studies. *Biophys. J*. 78:1400–1412.

Salamon, Z., H. A. Macleod, and G. Tollin. 1997a. Coupled plasmon-waveguide resonators: a new spectroscopic tool for probing proteolipid film structure and properties. *Biophys. J*. 73:2791–2797.

Salamon, Z., H. A. Macleod, and G. Tollin. 1997b. Surface plasmon resonance spectroscopy as a tool for investigating the biochemical and biophysical properties of membrane protein systems. I: Theoretical principles. *Biochim. Biophys. Acta*. 1331:117–129.

Salamon, Z., and G. Tollin. 1999a. Surface plasmon resonance, theory. *In* Encyclopedia of Spectroscopy and Spectrometry, Vol. 3. J. C. Lindon, G. E. Tranter, and J. L. Holmes. Academic Press, New York. 2311–2319.

Salamon, Z., and G. Tollin. 1999b. Surface plasmon resonance, applications. *In* Encyclopedia of Spectroscopy and Spectrometry, Vol. 3. J. C. Lindon, G. E. Tranter, and J. L. Holmes, editors. Academic Press, New York. 2294–2302.

Salamon, Z., and G. Tollin. 2000. Surface plasmon resonance spectroscopy in peptide and protein analysis. In Encyclopedia of Analytical Chemistry. R. A. Meyers, editor. John Wiley and Sons, Chichester, England. pp. 6050–6061.

Salamon, Z., and G. Tollin. 2001a. Plasmon resonance spectroscopy: probing molecular interactions at surfaces and interfaces. *Spectroscopy*. 15:161–175.

Salamon, Z., and G. Tollin. 2001b. Optical anisotropy in lipid bilayer membranes: coupled plasmon-waveguide resonance measurements of molecular orientation, polarizability, and shape. *Biophys. J*. 80:1557–1567.

Salamon, Z., and G. Tollin. 2002. Coupled plasmon-waveguide resonance spectroscopic device and method for measuring film properties in the ultraviolet and infrared special ranges. *U.S. Patent #: 6,421,128B1*.

Salamon, Z., G. Tollin, I. Stevenson, and D. Morton. 2002. Optical and electrical impedance spectroscopy studies of protein-lipid bilayer systems on a thin film coupled plasmon-waveguide resonator. *In* 45th Annual Technical Conference Proceedings, Society of Vacuum Coaters. Chicago, Illinois. 35–40.

Salamon, Z., Y. Wang, M. F. Brown, A. H. Macleod, and G. Tollin. 1994. Conformational changes in rhodopsin probed by surface plasmon resonance spectroscopy. *Biochemistry*. 33:13706–13711.

Salamon, Z., Y. Wang, J. L. Soulages, M. F. Brown, and G. Tollin. 1996. Surface plasmon resonance spectroscopy studies of membrane proteins: transducin binding and activation by rhodopsin monitored in thin membrane films. *Biophys. J*. 71:283–294.

Thoma, M., M. Schwendler, H. Baltes, C. A. Helm, T. Pfohl, H. Riegler, and H. Möhwald. 1996. Ellipsometry and x-ray reflectivity studies on monolayers of phosphatidylethanolamine and phosphatidylcholine in contact with *n*-dodecane, *n*-hexadecane, and bicyclohexyl. *Langmuir*. 12:1722–1728.

Thorén, P. E. G., D. Persson, M. Karlsson, and B. Nordén. 2000. The Antennapedia peptide penetratin translocates across lipid bilayers—the first direct observation. *FEBS Lett*. 482:265–268.

White, S. H. 1986. The physical nature of planar bilayer membranes. *In* Ion Channel Reconstitution. C. H. Miller, editor. Plenum Publishing Corporation, New York. pp. 3–35.